Determination of Exciton Reduced Mass and Gyromagnetic Factor of Wurtzite (InGa)As Nanowires by Photoluminescence Spectroscopy under High Magnetic Fields

Marta De Luca,[†] Antonio Polimeni,[†,*] Mario Capizzi,[†] Alan J. Meaney,[‡] Peter C. M. Christianen,[‡] Jan Kees Maan,[‡] Francesco Mura,[§] Silvia Rubini,[∥] and Faustino Martelli[⊥,*]

[†]Dipartimento di Fisica and CNISM, Sapienza Università di Roma, Piazzale A. Moro 2, 00185 Roma, Italy, [‡]High Field Magnet Laboratory, Institute of Molecules and Materials, Radboud University Nijmegen, Toernooiveld 7, NL-6525 ED Nijmegen, The Netherlands, [§]Dipartimento di Scienze di Base e Applicate per l'Ingegneria, Sapienza Università di Roma, Via Scarpa 16, 00185 Roma, Italy, [∥]TASC-IOM-CNR, Area Science Park, S.S. 14, Km. 163.5, 34012 Trieste, Italy, and [⊥]IMM-CNR, Via del Fosso del Cavaliere 100, 00133 Roma, Italy

ABSTRACT Semiconductor nanowires (NWs) have the prospect of being employed as basic units for nanoscale devices and circuits. However, the impact of their one-dimensional geometry and peculiar crystal phase on transport and spin characteristics remains largely unknown. We determine the exciton reduced mass and gyromagnetic factor of (InGa)As NWs in the wurtzite phase by photoluminescence (PL) spectroscopy under very high magnetic fields. For B perpendicular to the NW $\hat{c}$ axis, the exciton reduced mass is 10% greater than that expected for the zincblende phase and no field-induced circular polarization of PL is observed. For B parallel to $\hat{c}$, an exciton reduced mass 35% greater than that of the zincblende phase is derived. Moreover, a circular dichroism of 70% is found at 28 T. Finally, an analysis of the PL line shape points at two Zeeman split levels, whose separation corresponds to an exciton gyromagnetic factor $|g_e - g_{h,||}| = 5.8$. These results provide a quantitative estimate of the basic electronic and spin properties of NWs and may guide a theoretical analysis of the band structure of these fascinating nanostructures.

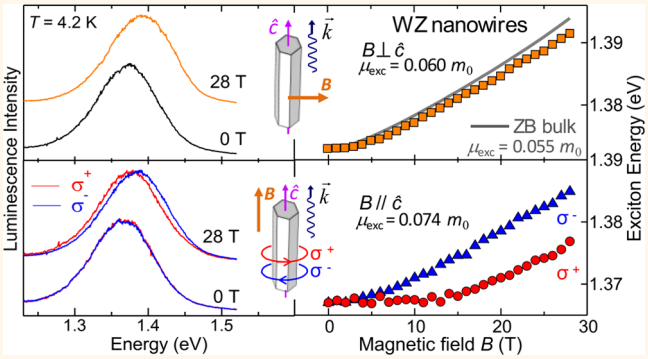

KEYWORDS: semiconductor nanowires · magneto-photoluminescence · exciton · effective mass · gyromagnetic factor · wurtzite phase

Semiconductor nanowires (NWs) have diameters of about 100 nm or less, and are up to several micrometers in length. The formation of NWs occurs for almost any semiconductor material,[1] and their properties are exploitable in a large number of applications.[2] For NWs to be useful, a full understanding of their electronic properties is required, including their complex lattice and band structure. For III−V compounds, such as GaAs, InAs, and InP—and related alloys—, an hexagonal wurtzite (WZ) phase is routinely found in Au-seeded NWs, but single pure-phase NWs are hardly obtained.[3] An experimental assessment of the electronic properties of NWs is, therefore, rather difficult as shown by the continuing debate regarding the precise value of the WZ GaAs band gap energy.[4] The carrier effective mass is also unknown, despite its relevance for the transport performances.

The main changes in the band structure of III−V's on going from zincblende (ZB) to WZ phase are the following:[5−8] (i) a valence band (VB) splitting, due to the lowered spatial symmetry of the WZ phase, that adds to the spin−orbit effect and leads to a VB energy ladder Γ_9^V, Γ_{7u}^V, and Γ_{7l}^V (from shallower to deeper states); (ii) the presence of a

* Address correspondence to antonio.polimeni@roma1.infn.it, faustino.martelli@cnr.it.

Received for review July 10, 2013 and accepted November 21, 2013.

Published online November 21, 2013
10.1021/nn405743t

Γ_8^C conduction band (CB) at energy higher[8] (or lower)[7,9] than that of the Γ_7^C CB, depending on the material system and strain.[8] This additional CB is due to a zone folding along the [0001] direction in the real space, or $\hat{c}$ axis, arising from a WZ unit cell longer than that of ZB. The electron effective mass at Γ_8^C is expected to be considerably heavier than that at Γ_7^C.[7,8,10]

Photoluminescence (PL),[11,12] PL excitation,[4,13] photocurrent,[14] and Raman scattering[10,15] experiments have provided valuable information on the NW band structure. Indeed, those optical techniques involve interband transitions whose intensity is ruled by polarization-related selection rules very sensitive to the crystal symmetry.[5,16] Magneto-optical studies can give insight also into the transport (*e.g.*, carrier effective mass) and spin (*e.g.*, carrier gyromagnetic factor) properties of NWs, whose symmetry might be addressed by different NW/magnetic-field geometrical configurations. Magneto-PL measurements have been recently used to characterize the optical quality and the electronic structure of GaAs/AlAs core/shell ZB NWs[17] and WZ/ZB quantum disks in GaAs NWs,[18] respectively. Magneto-PL studies have been also employed in II−Mn−VI NWs to address the sp−d coupling induced by Mn atoms in these nanostructures.[19,20]

In this paper, we report on the electronic properties of $In_{0.10}Ga_{0.90}As$ NWs grown on GaAs(111) substrates. Low-temperature PL recorded on a NW ensemble at zero magnetic field shows a remarkably high (~90%) degree of linear polarization *perpendicular* to the wire $\hat{c}$ axis, indicating a predominant WZ phase. The application of a magnetic field along different directions with respect to the $\hat{c}$ axis shows marked anisotropies in the exciton reduced mass, Zeeman splitting, and circular dichroism of the emitted light. A quantitative analysis of the experimental data permits us to determine the exciton reduced mass and gyromagnetic factor, thus prompting a comparison to band structure calculations.

We review first the main characteristics of excitons in WZ crystals. The energy ordering and symmetry of exciton levels involving different nondegenerate valence bands in bulk WZ CdS was established by Thomas and Hopfield.[21] A similar picture applies to other WZ-phase materials, *e.g.*, GaN, CdSe, and ZnO, and most likely holds also for NWs, whenever their size allows neglecting carrier quantum confinement. For a Γ_8^C CB minimum at energy higher than the Γ_7^C minimum, the first three exciton states are associated to the $\Gamma_7^C \leftrightarrow \Gamma_9^V$ or A, $\Gamma_7^C \leftrightarrow \Gamma_{7u}^V$ or B, and $\Gamma_7^C \leftrightarrow \Gamma_{7l}^V$ or C transitions, in order of increasing energy; see left panel in Figure 1. Admixing effects between the different VBs in the exciton states can be neglected when these bands differ in energy much more than the exciton binding energy. This is the case of excitons in InP[13] and GaAs[4] NWs, where the Γ_9^V and Γ_{7u}^V extrema are separated by ~40 and ~110 meV, respectively, and, hence, of excitons in (InGa)As NWs with 10% of In.

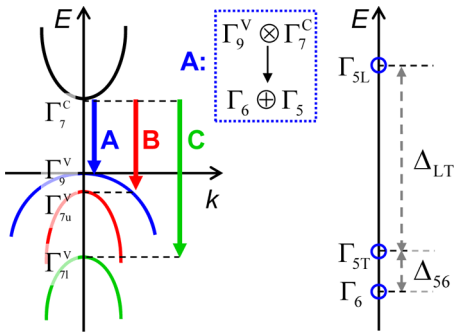

Figure 1. (Left) Simplified sketch of transitions from the lowest conduction band to the three WZ valence bands. Conduction- and valence-band symmetries at Γ point, transition labels, and group symmetry transformations are indicated. (Right) Excitonic levels and relative energy ordering for the A exciton. The energy splittings Δ_{56} and Δ_{LT} are discussed in the text.

In this work, we focus on the lowest energy transition A, which dominates the PL spectra. On the grounds of group theory, A excitons divide into twofold degenerate Γ_5 and Γ_6 states[22]

$$\Gamma_7 \otimes \Gamma_9 \rightarrow \Gamma_5 \oplus \Gamma_6 \quad (1)$$

where only Γ_5 excitons can be optically observed in a dipole approximation, with resulting light polarization $\hat{\varepsilon} \perp \hat{c}$.[22] We refer to dipole-allowed Γ_5 excitons, with energy E_5, as 'bright' excitons and to dipole-forbidden Γ_6 excitons, with energy E_6, as 'dark' excitons. Dark and bright excitons differ by $\Delta_{56} = E_5 - E_6$ that is the analytic part of the electron−hole exchange interaction.[23,24] This energy is very small in bulk systems (0.2 meV in CdS[24] and 0.12 meV in GaN[25]) and is sizable, instead, in WZ nanocrystals. Therein, it depends on size (≈10 meV for a nanocrystal radius of about 3 nm)[26] and leads to a five-level exciton "fine structure" with states characterized by the projection along $\hat{c}$ of the total angular momentum. In the nanowires investigated here [diameter ~60 nm and length in excess of 1 μm; see Figure 2b and 3a], both exchange interactions and quantum confinement can be considered small.

For an exciton with wavevector $k \perp \hat{c}$, the Γ_5 excitons are split in transverse (Γ_{5T}) and longitudinal (Γ_{5L}) states by the nonanalytic part of the electron−hole exchange interaction, $\Delta_{LT} = E_{5L} - E_{5T}$. Γ_{5L} states are forbidden in a dipole approximation.[23,24,27] In our WZ $In_{0.1}Ga_{0.9}As$ nanowires, Δ_{LT} should be within the values it has in ZB GaAs (0.08 meV)[28] and in WZ GaN (1 meV).[25] For $k \parallel \hat{c}$, Δ_{LT} reduces to zero.[27] The excitonic levels existing at null magnetic field for a generic direction of k are sketched in the right panel of Figure 1. The effect of a magnetic field on the above-mentioned states will be discussed in the following.

RESULTS AND DISCUSSION

Zero Magnetic Field. Figure 2a shows the $T = 10$ K PL spectra of an ensemble of $In_{0.1}Ga_{0.9}As$ NWs recorded

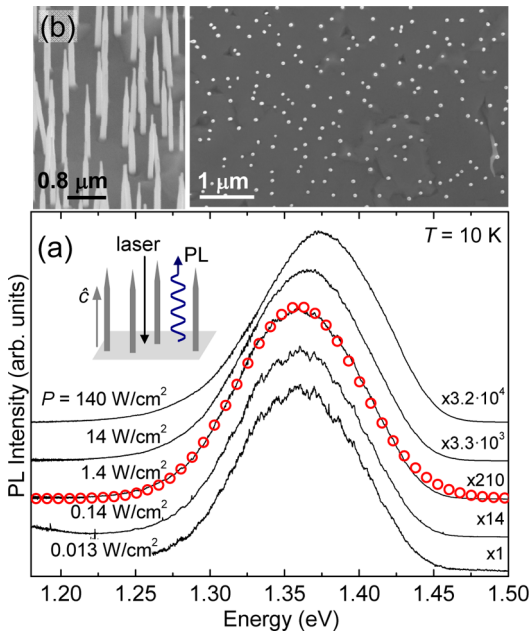

Figure 2. (a) Normalized PL spectra of an ensemble of $In_{0.1}Ga_{0.9}As$ nanowires at $T = 10$ K for different laser power densities, P. Intensity multiplication factors are shown. Open symbols in the middle spectrum are a Gaussian fit to the data. The measurements were performed in a backscattering configuration: laser and luminescence directions are both perpendicular to the substrate and antiparallel each other, as depicted in the inset. (b) SEM images of the sample, whose PL spectra are shown in panel a. Left and right images were taken in side- and planar-view modes, respectively.

for excitation power densities, P, varied by about a factor 10^4. A backscattering configuration was used, with laser excitation and luminescence emission traveling in opposite directions and orthogonal to the sample substrate (namely, parallel to the NW $\hat{c}$ axis; see inset).

In this case $k \parallel \hat{c}$ and transitions from the Γ_5 exciton state are observed, being Γ_6 excitons dipole-forbidden. The PL line shape is Gaussian-like with a full-width at half-maximum of 100 meV, see open symbols in the middle spectrum in Figure 2a. Despite the compositional inhomogeneity resulting from a gradient in the In concentration within each wire,[29,30] the investigated NWs present a high degree of directional ordering as displayed by the scanning electron microscopy (SEM) images in Figure 2b. We notice that the PL line shape remains unchanged in the investigated range of laser power densities (more than 4 orders of magnitude), except for a rigid blue-shift (~10 meV) at the highest P. This behavior indicates that the contribution from impurity states to the PL band is small. This band is attributed to excitonic recombination, as supported also by magnetic field studies. Finally, the absence of a large, continuous blue-shift of the PL peak energy with increasing P indicates that contributions from type-II ZB-WZ transitions are negligible.[31,32]

The high morphological ordering in the NW array is reflected by the noticeable degree of PL anisotropy observed in these WZ nanostructures, where well-defined polarization selection rules are predicted.[16] Figure 3a shows the PL spectra obtained by exciting the nanowire ensemble with an incident laser beam parallel to the NW $\hat{c}$ axis, while the emitted light was detected *alongside* the NWs; see bottom left inset. Dipole-allowed transitions from Γ_5 states should be strongly anisotropic because they can be observed only for polarization $\hat{\varepsilon} \perp \hat{c}$.[4,11] In order to evaluate this anisotropy, luminescence was filtered by a linear polarizer, whose permissive axis was rotated to form different angles α with the $\hat{c}$ axis; see sketch in the top inset in Figure 3a. The weak band at high energy (~1.49 eV) is due to the GaAs substrate and is completely unpolarized, while the more intense NW emission at 1.36 eV is strongly linearly polarized. Figure 3b displays a polar plot of the NW PL intensity exhibiting a maximum when the luminescence polarization vector $\hat{\varepsilon}$ is perpendicular to the NW axis ($\alpha = 90°$ and 270°, namely, $\hat{\varepsilon} \perp \hat{c}$). The resulting nearly 90% degree of linear polarization shows that the NWs are predominantly in the WZ phase[4,11] and that their alignment uniformity is extremely high (nearly 3×10^5 wires are probed at once in our experiment). The effective polarization perpendicular to the wires is even greater than 90% if the "antenna effect", which makes PL emission polarized along the NW axis,[33] is taken into account.

It is worth mentioning that the symmetry of the lowest conduction band cannot be established on the ground of polarization-resolved measurements. In fact, polarization selection rules predict that transitions involving the Γ_9^V state and either the Γ_7^C or Γ_8^C states, namely, the two lowest CB energy states in WZ,[7,8] are both dipole-allowed only for photon polarization perpendicular to the $\hat{c}$ axis.[16] Our magnetic field studies indicate that the lowest CB has a Γ_7^C symmetry character instead of Γ_8^C.

Magnetic Field >0 T. A magnetic field has two main effects on the exciton states. The first effect, referred to as diamagnetic shift ΔE_d, is an increase in the exciton energy, whose extent and functional variation with B depend essentially on the relative strength between the "magnetic energy" (gauged by $\hbar\omega_c/2 \approx 6 \times 10^{-5} B/\mu_{exc}$ eV, where μ_{exc} is the exciton reduced mass) and the exciton binding energy ($E_b^{exc} = 13.6\ \mu_{exc}/\varepsilon_r^2$ eV, where ε_r is the relative dielectric constant).[34] In $In_{0.1}Ga_{0.9}As$ ($\varepsilon_r = 12.7$ and $\mu_{exc} = 0.055\ m_0$ for the ZB phase),[35] these energies are comparable [$E_b^{exc} \approx 5$ meV and $\hbar\omega_c$ (28 T)/2 ≈ 30 meV] and a perturbative approach cannot be employed. A variational technique is more suitable, instead, leading to[36−38]

$$\Delta E_d(B) = 13.6 \times 10^3 \left(\frac{(\mu_{exc}/m_0)}{\varepsilon_r^2}\right) \cdot \sum_{p=1}^{9} A_p \left[4.26 \times 10^{-6} \cdot \left(\frac{\varepsilon_r}{(\mu_{exc}/m_0)}\right)^2 B\right]^p \text{ meV} \quad (2)$$

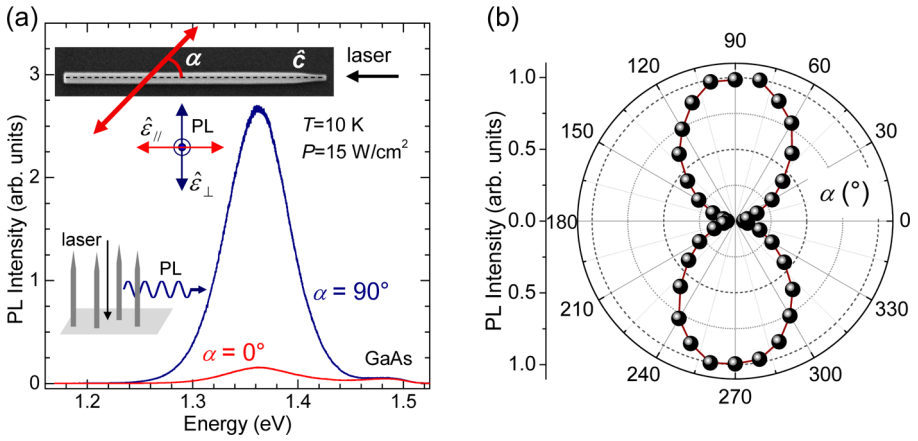

Figure 3. (a) PL spectra at T = 10 K of an ensemble of $In_{0.1}Ga_{0.9}As$ nanowires recorded for different orientations of luminescence polarization vector $\hat{\varepsilon}$ with respect to the NW $\hat{c}$ axis. "GaAs" indicates emission from the substrate. The bottom inset sketches the experimental configuration employed. The wire shown in the top inset is a SEM image recorded on a 1.3 μm-long wire singled out from the NW ensemble studied. In this scheme, the luminescence points toward the reader and is filtered by a linear polarizer (double-arrowed line) oriented at various angles with respect to the nanowire long axis. Labels $\alpha = 0°$ and 90° correspond to emission polarized parallel and orthogonal to the NW axis, respectively. (b) Polar plot of the dependence of PL intensity on α.

where A_p are coefficients determined by a numerical solution to the problem.[37]

The second effect of a magnetic field is a Zeeman splitting (ZS), whose expression involves the carrier gyromagnetic factor. In the following, g_h and g_e will be the hole and electron g-factors, respectively, and g_{exc} the g-factor of the resulting exciton. In WZ bulk crystals, $g_h = g_{h,\parallel} \cos \vartheta$, where ϑ is the angle between the magnetic field B and the $\hat{c}$ axis and $g_{h,\parallel}$ is the component of g_h parallel to the field. Therefore, g_h is null when the magnetic field is perpendicular to $\hat{c}$, while $g_e (= g_{e,\perp} = g_{e,\parallel})$ is isotropic.[25,39] We point out that this scenario changes completely in WZ nanocrystals, where the strong exchange interaction "binds" electron and hole spin-projections and impedes to consider g_h and g_e separately.[40] At variance with bulk WZ, in nanocrystals the Zeeman splitting is ruled by an effective g-factor and is given by $ZS = g_{exc}\mu_B B \cos \vartheta$ (where μ_B is the Bohr magneton), which is null when the magnetic field is perpendicular to the $\hat{c}$ axis (even if $g_{exc} \neq 0$).[41]

Notice that all our measurements have been performed with emitted light (and exciton) wavevector $k \parallel \hat{c}$. Then, we discuss this case only and report the calculated energies of the ground-state of A excitons in bulk WZ for two different orientations of the magnetic field.[24,27,42]

$B \parallel \hat{c}$

A magnetic field parallel to the $\hat{c}$ axis does not perturb the crystal symmetry and, therefore, does not mix bright and dark excitons. The B-dependence of the exciton states is[24,27,42]

$$\begin{aligned} E_5^{\pm}(B) &= E_0 + \Delta_{56} + \Delta E_{d,\parallel}(B) \pm \frac{1}{2}|g_e - g_{h,\parallel}|\mu_B B \\ E_6^{\pm}(B) &= E_0 + \Delta E_{d,\parallel}(B) \pm \frac{1}{2}|g_e + g_{h,\parallel}|\mu_B B \end{aligned} \quad (3)$$

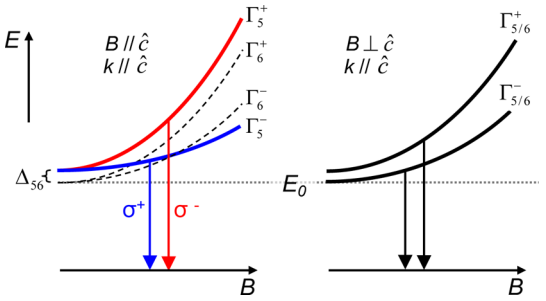

Figure 4. Magnetic field dependence of the lowest energy exciton levels involved in transition A. The curved lines mimic the effect of diamagnetism and Zeeman splitting on those levels (for $B \parallel \hat{c}$ on the left, and for $B \perp \hat{c}$ on the right; in both cases $k \parallel \hat{c}$). In the left panel, solid and dashed curves refer to bright (Γ_5) and dark (Γ_6) excitons, respectively. The vertical arrows indicate the exciton recombination toward the ground state for the given circular polarization status of the emitted photon. The Zeeman splitting of Γ_5 states is larger than that of Γ_6 states because opposite signs for g_e and $g_{h,\parallel}$ have been assumed. In the right panel, solid curves refer to mixed $\Gamma_{5/6}$ excitons. The vertical arrows indicate that exciton recombination may occur from both mixed states. The dashed horizontal line marks the reference E_0 level.

where E_0 is the energy of the unperturbed Γ_6 state. For $B = 0$, $E_6^{\pm} = E_0 = E_6$ and $E_5^{\pm} = E_6 + \Delta_{56}$, as shown in the right panel of Figure 1 for $\Delta_{LT} = 0$, *i.e.* $k \parallel \hat{c}$. For $B \neq 0$, a diamagnetic shift $\Delta E_{d,\parallel}(B)$ and a linear Zeeman splitting occur. The projection of the total angular momentum on the $\hat{c}$ axis is a good quantum number and all transitions have a well-defined behavior when observed with circularly polarized light (see left panel in Figure 4).[27,42]

$B \perp \hat{c}$

A magnetic field perpendicular to the $\hat{c}$ axis lowers the crystal symmetry and mixes bright and dark excitons, thus creating two doubly degenerate $\Gamma_{5/6}$ states with total energies:[24,27,42]

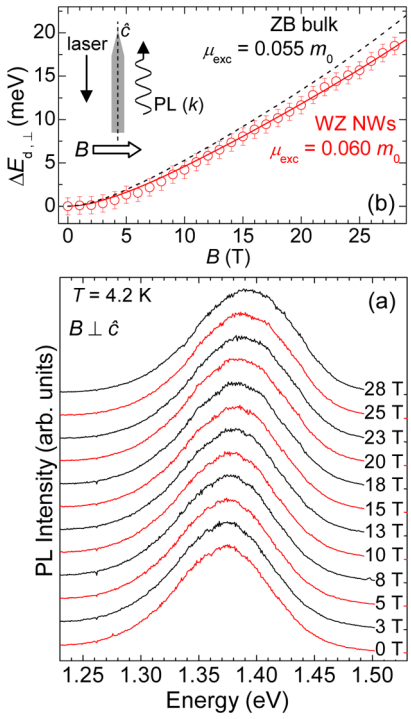

Figure 5. (a) T = 4.2 K peak-normalized PL spectra of an ensemble of $In_{0.1}Ga_{0.9}As$ nanowires for different values of the magnetic field. Laser power density P = 1.3 kW/cm^2. The field direction is perpendicular to the NW long axis, $\hat{c}$. The experimental configuration is sketched in panel b. (b) Magnetic field dependence of the PL peak energy of the exciton band (symbols). The solid line is a fit of eq 2 to the data. The dashed line is the diamagnetic shift expected by the same equation for an exciton having the reduced mass of bulk ZB $In_{0.1}Ga_{0.9}As$.

$$E^{\pm}_{5/6}(B) = E_0 + \frac{1}{2}\Delta_{56} + \Delta E_{d,\perp}(B) \pm \frac{1}{2}[\Delta^2_{56} + g_e^2\mu_B^2B^2]^{1/2} \quad (4)$$

Here, the energy does not depend on g_h, which is zero because $\cos\vartheta = 0$. For $B = 0$, $E_{5/6} = E_0 = E_6$ and $E^{\perp}_{5/6} = E_6 + \Delta_{56}$. The right panel in Figure 4 sketches the energy variation of the exciton levels for $B\perp\hat{c}$ and $k \parallel \hat{c}$. As can be seen in eq 4, the Zeeman splitting of $\Gamma_{5/6}$ states can be considered linear only if $\Delta_{56} \ll \mu_B Bg_e$.

We now present magneto-PL data in our highly oriented NW ensemble. We expect very different results for B being parallel or orthogonal to $\hat{c}$, contrary to the case of ensembles of WZ nanocrystals,[26,43,44] where the $\hat{c}$ axis takes all possible orientations.

Voigt Configuration ($B \perp k \parallel \hat{c}$). Figure 5a shows some PL spectra taken in the Voigt configuration for magnetic fields up to 28 T. The exciting laser and luminescence directions are antiparallel and both directed along the $\hat{c}$ axis. The field is orthogonal to those directions, as sketched in the inset in Figure 5b.

This configuration gives rise to mixed $\Gamma_{5/6}$ states and to a non linear Zeeman splitting between them [see right panel in Figure 4 and eq 4]. These mixed states have been observed for B > 8 T and $k\perp\hat{c}$ in WZ GaN, where the exciton PL line width is ~2 meV and Δ_{LT} = 1 meV.[25] On the contrary, in our samples the PL line shape remains nearly unchanged with increasing magnetic field, but for a slight broadening. This broadening, which increases progressively with magnetic field and is equal to ~7 meV at 28 T (see Figure 6), is most likely due to the splitting of the mixed $\Gamma_{5/6}$ state induced by the magnetic field and reported in eq 4.

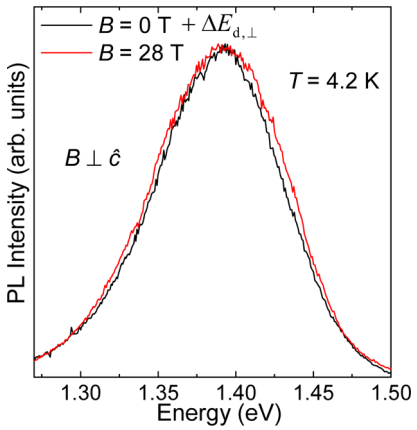

Figure 6. T = 4.2 K peak-normalized PL spectra already shown in Figure 5a. Red and black lines refer to PL spectra recorded at 28 and at 0 T, respectively. The B = 0 T spectrum has been blue-shifted by $\Delta E_{d,\perp}$ = 18.5 meV in order to overlap with the B = 28 T spectrum. This latter is ~7 meV broader than the B = 0 T spectrum. The experimental configuration is depicted in the inset of Figure 5b.

A fit of the PL line shape in terms of the two contributions $E^{\pm}_{5/6}$ could allow determining the values of Δ_{56} and g_e. Those fitted values, however, have an exceedingly high uncertainty because of a PL line width much larger than the Zeeman splitting. Therefore, we will analyze the two mixed $\Gamma^{\pm}_{5/6}$ states as degenerate at all magnetic fields and shifting all together according to the diamagnetic term $\Delta E_{d,\perp}$; see eq 4. This shift, as derived from a Gaussian fit to the PL spectra at all fields (not shown), is displayed in Figure 5b as a function of B.

The initial (B < 15 T) quadratic-like dependence of $\Delta E_{d,\perp}$ on B turns into a linear-like dependence at higher fields, a signature of excitonic recombination.[34,36−38] The reduced mass governing the diamagnetic shift for $B\perp\hat{c}$ corresponds to exciton motion in a plane containing the [0001] direction, thus a combination of carrier mass parallel and orthogonal to $\hat{c}$.[45] We name this mass $\mu^{\perp\parallel}_{exc}$ and find it equal to 0.060 m_0 by eq 2 displayed as solid line in Figure 5 (b). This value can be compared with the exciton mass expected in bulk ZB $In_{0.10}Ga_{0.90}As$ (μ_{exc} = 0.055 m_0, as obtained by a linear interpolation between the effective masses of the ZB InAs and GaAs end compounds; see ref 35) leading to the dashed line in Figure 5b. Note that the band gap of WZ is usually larger than that of ZB,[4,46] leading here to an underestimation of the In concentration and, hence, to an overestimation of the carrier effective mass of ZB.

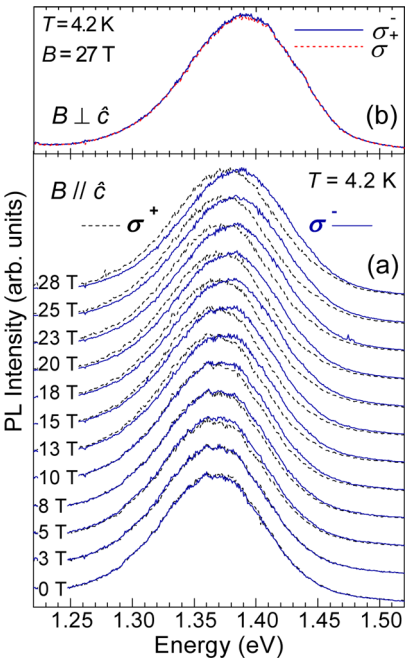

Figure 7. (a) T = 4.2 K peak-normalized PL spectra of an ensemble of $In_{0.1}Ga_{0.9}As$ nanowires for different values of magnetic field $B \parallel \hat{c}$. P = 1.1 kW/cm^2. Solid and dashed lines refer to σ^- and σ^+ circular polarization, respectively. The experimental configuration is depicted in Figure 8a. (b) T = 4.2 K PL spectra of the same ensemble of $In_{0.1}Ga_{0.9}As$ nanowires, recorded at a magnetic field $B \perp \hat{c}$ of 27 T. P = 1.3 kW/cm^2. Solid and dashed lines refer to opposite circular polarization status. At variance with $B \parallel \hat{c}$, the two spectra overlap. The experimental configuration is depicted in the inset of Figure 5b.

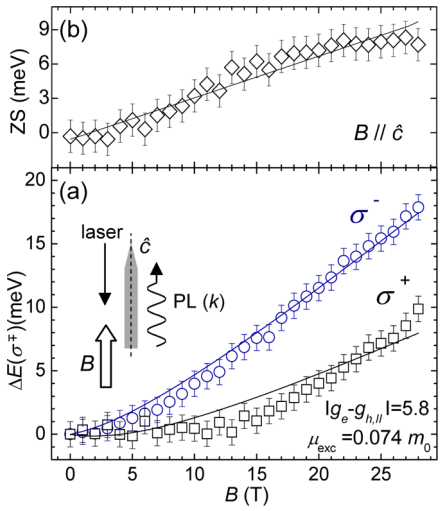

Figure 8. (a) Magnetic field dependence of the PL peak energy, open symbols, of the $\Gamma_5^{\pm}$ exciton bands for opposite circular polarization components. The solid lines are a fit of eq 5 to the exciton energies. The inset depicts the experimental configuration in which the laser, PL direction, and magnetic field are (anti-) parallel each other. (b) Magnetic field dependence of the Zeeman splitting (open symbols). The solid line is the difference between the fitting curves shown in panel a.

The estimated $\mu_{exc}^{\perp,\parallel}$ = 0.060 m_0 value is, therefore, at least 10% higher than that of ZB.

Faraday Configuration ($B \parallel k \parallel \hat{c}$). In this configuration, the laser, luminescence, and $\hat{c}$ axis directions are the same as for the Voigt configuration, but the magnetic field is oriented parallel to the $\hat{c}$ axis and to the wavevector k of the emitted photons; see inset in Figure 8a. Γ_5 and Γ_6 states shift and split as reported by eq 3,[24,27,42] with opposite circularly polarized light emission from the two Zeeman split states; see left panel in Figure 4. The magneto-PL spectra of our $In_{0.10}Ga_{0.90}As$ NWs, recorded in Faraday geometry for left (σ^+) and right (σ^-) circular polarizations, are shown in Figure 7a. We attribute PL emission at zero field to the bright exciton Γ_5. As soon as the magnetic field is turned on, circular polarization-resolved measurements unveil the $\Gamma_5^{\pm}$ Zeeman states, which separate progressively for increasing magnetic field. For both circular polarizations, the PL lineshapes do not broaden with increasing B (contrary to Figure 6). However, the intensity of the two transitions with opposite circular polarization varies in a quite different way resulting in a marked circular dichroism, as detailed in the following. Instead, in the Voigt configuration the intensity and peak position of the spectra at a same field recorded with σ^+ and σ^- polarization are still identical up to 27 T (see Figure 7b). This anisotropy in the magneto-optical properties is typical of WZ phase materials, where marked circular dichroism can be observed only in a Faraday configuration.

Let us now analyze the results displayed in Figure 7. In the present bulk-like WZ NWs, the extent of exciton diamagnetic shift and Zeeman splitting is comparable, contrary to the case of WZ nanocrystals where the strong carrier confinement results in a negligible diamagnetic shift.[26,44,47] For that reason, the analysis of our magneto-PL spectra is not straightforward. The peak energy difference between σ^- and σ^+ PL spectra is the ZS of the Γ_5 exciton, with σ^- transitions at energy higher than σ^+ transitions, as anticipated in the left panel in Figure 4. Figure 8a shows the shift of the PL peak energy, $\Delta E(\sigma^{\mp})$, for σ^+ (squares) and σ^- (circles) polarizations (as determined by a Gaussian fit, not shown) as a function of B:

$$\Delta E(\sigma^{\mp}) = E_5^{\pm}(B) - E_5^{\pm}(0)$$
$$= \Delta E_{d,\parallel}(\mu_{exc}) \pm \frac{1}{2}|g_e - g_{h,\parallel}|\mu_B B \qquad (5)$$

where the first term on the right-hand side is given by eq 2 and the second term accounts for the ZS; see eq 3. A fit of eq 5 (solid lines) to the two sets of data allows us to estimate $|g_e - g_{h,\parallel}|$ and μ_{exc}. In this case, we refer to the reduced exciton mass as $\mu_{exc}^{\perp}$ because this configuration gives access to the carrier mass in the plane perpendicular to $\hat{c}$.

The fit results are $\mu_{exc}^{\perp}$ = 0.074 m_0, a value sizably larger than that found for $B \perp \hat{c}$ ($\mu_{exc}^{\perp,\parallel}$ = 0.060 m_0), and $|g_e - g_{h,\parallel}|$ = 5.8, as derived in Figure 8a. The experimental Zeeman splitting is shown in Figure 8b (open symbols).

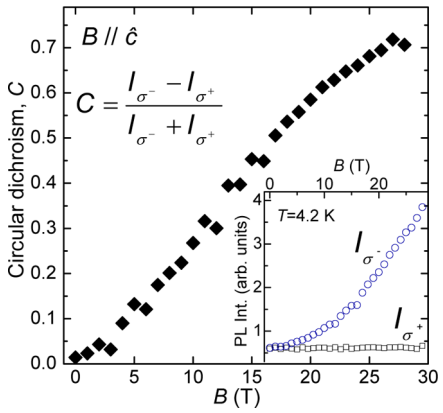

Figure 9. Magnetic field dependence of the PL circular dichroism degree for $B \| \hat{c}$. The inset shows the PL intensity dependence on B for the two circular polarizations.

The solid line represents the equation ZS = $|g_e - g_{h\|}|\mu_B B$, with $|g_e - g_{h\|}| = 5.8$. The poor linear dependence on B of the experimental Zeeman splitting follows the not fully satisfactory fits of the dependence on magnetic field of the PL peak energies shown in Figure 8a. A nonlinear dependence of ZS on B could be ascribed to a field-dependent value of the carrier g-factor, as it has been reported for (InGa)As/GaAs quantum wells[48] and asymmetric GaAs/AlAs quantum wells.[49] More likely, it could also be due to contributions from Γ_6 states, whose energy is quite close to the energy of Γ_5 states, in particular at low magnetic fields. PL emission from those states, although dipole-forbidden, has been already observed, indeed, in the configuration $B \| \hat{c}$.[25,27] Moreover, the energy of Γ_5^- state would be slightly higher than that of Γ_6^- states, if g_e and $g_{h\|}$ had opposite signs as in bulk GaAs;[50] see left panel in Figure 4. In this case, contributions from Γ_6^- states could account for the almost constant value of $\Delta E(\sigma^+)$ at low fields displayed in Figure 8a and for the ensuing non linear dependence of the Zeeman splitting.

Figure 9 shows the B-dependence of the degree of PL circular dichroism $C = (I_{\sigma^-} - I_{\sigma^+})/(I_{\sigma^-} + I_{\sigma^+})$, where $I_{\sigma^\pm}$ is the PL intensity measured for the two circular polarizations. The variation in I_{σ^+} with B is displayed in the inset. A steady increase in C is observed up to 20 T followed by a slow-down at higher fields, where $C > 70\%$. It is quite surprising that emission from the higher energy state (Γ_5^+, observed with σ^- polarization) is more intense than the emission from the lower Γ_5^- state (observed with σ^+ polarization). This anomalous behavior has been also observed in WZ GaN.[51]

Discussion of Results. The quantitative analysis of the diamagnetic shift for different orientations between applied field and $\hat{c}$ axis reveals a carrier mass anisotropy in WZ NWs: $\mu_{exc}^{\perp\|}$ (=0.060 m_0) < $\mu_{exc}^{\perp}$ (=0.074m_0). In Faraday configuration, the carrier mass m^* probed by the magnetic field is that perpendicular to the WZ axis, while in Voigt configuration, it results from an averaged contribution $m^* = (m_\| \cdot m_\perp)^{1/2}$ of the carrier mass parallel ($m_\|$) and orthogonal ($m_\perp$) to $\hat{c}$.[45] Electron and hole mass contributions cannot be separated in μ_{exc}, and therefore, it is not possible at this stage to determine independently the degree of anisotropy of the conduction and valence band transport properties. The exciton reduced mass is heavier than that expected in ZB (μ_{exc} = 0.055 m_0 for bulk $In_{0.1}Ga_{0.9}As$). This latter finding can be attributed to a lower energy dispersion acquired by the CB as a consequence of the first Brillouin zone folding. The values we find suggest, however, that the effective mass increase is more compatible with a CB minimum having a Γ_7^C rather than Γ_8^C character, since in the latter case much heavier masses are predicted.[7,8]

As regards the Zeeman splitting, it cannot be estimated in the $B \perp \hat{c}$ configuration because of the broadness of the PL spectra. On the contrary, in the $B \| \hat{c}$ configuration, measurements performed with circularly polarized light allow determining the ZS and the effective exciton gyromagnetic factor $|g_e - g_{h\|}| = 5.8$. This value can be compared only with that estimated for bulk ZB $In_{0.1}Ga_{0.9}As$ by using the Luttinger parameter $\tilde{k}$ reported in literature ($g_{exc} = -1/4g_e - 5/2\tilde{k} = -4.1$).[50,52] In Faraday geometry, the observed non linear dependence of Zeeman splitting on B is discussed in terms of possible contributions from Γ_6 states.

Finally, we note that the dependence of the PL intensity of the σ^- and σ^+ components on increasing magnetic field is quite different from that found in WZ nanocrystals. Therein, the PL intensity of the two circular polarization increases (σ^-) or decreases (σ^+) with B until they both saturate.[26,47,53] In present NWs, σ^+ does not change with field, while σ^- increases steadily without showing any plateau (see inset in Figure 9) suggesting that the spin system does not reach thermal equilibrium. This different behavior between nanocrystals and NWs could be related to the increase in PL intensity that a magnetic field induces on loosely bound electron–hole pairs forming in bulk materials or relatively large nanostructures.[54] Indeed, B determines an increase in wave function overlap between charge carriers that results in a greater recombination rate opposing to nonradiative decay paths always present in real materials. This additional effect scrambles the dependences expected for σ^- and σ^+ polarizations. No such an effect is expected in already tightly bound excitons like those forming in nanocrystals.

CONCLUSIONS

Photoluminescence measurements at low temperature as a function of magnetic field up to 28 T have been used to study the fundamental electronic properties of an ensemble of $In_{0.1}Ga_{0.9}As$ nanowires with

hexagonal structure. The NW luminescence exhibits a degree of linear polarization as high as ~90% at zero field, with polarization vector orthogonal to the NW axis, a distinctive feature of the wurtzite phase. The marked anisotropy of the NW optical properties is also apparent from magneto-PL measurements. Indeed, application of a magnetic field perpendicular or parallel to the NW $\hat{c}$ axis results in largely different values of the exciton diamagnetic shift, Zeeman splitting, and PL circular dichroism. For $B \perp \hat{c}$, we derive an exciton reduced mass $\mu_{exc}^{\perp\parallel} = 0.060\ m_0$ and observe no circular dichroism in PL emission. An indication of the Zeeman splitting of the mixed bright and dark exciton states induced by the magnetic field is provided by the increasing broadening of PL spectra for increasing B. For $B \parallel \hat{c}$, we derive $\mu_{exc}^{\perp} = 0.074\ m_0$, an exciton gyromagnetic factor $|g_e - g_{h\parallel}| = 5.8$, and find a >70% circular dichroism of the emitted light. The increase in carrier effective mass with respect to zincblende is in qualitative agreement with theoretical expectations in various materials[7,8,55] and provides valuable hints concerning the symmetry character of the conduction band minimum.

METHODS

(InGa)As, NWs, were grown on a deoxidized GaAs (111)B substrate by solid-source molecular beam epitaxy. Gold particles were used as seeds for the NW growth at 500 °C.[30] We estimate an average In composition equal to 0.10 by the known compositional dependence of the band gap energy in bulk unstrained ZB (InGa)As.[35] The lattice structure of the nanowires is dominated by the wurtzite phase.[29,30] For PL measurements, samples were maintained at $T = 10$ K by using a closed-cycle cryostat and excited by a frequency-doubled Nd:YVO_4 laser ($\lambda_{exc} = 532$ nm, laser spot radius ~100 μm). The emitted light was spectrally analyzed by a 0.75 m long monochromator (spectral resolution equal to 0.12 meV) and detected by a N-cooled Si CCD. PL measurements under magnetic fields up to 28, performed in a water-cooled Bitter magnet with samples kept at $T = 4.2$ K in a liquid He-bath cryostat, were excited by a frequency-doubled Nd:YVO_4 laser (laser spot radius ~5 μm) and spectrally analyzed by a 0.30 m long monochromator (spectral resolution equal to 0.6 meV) equipped with a N-cooled Si CCD. The analysis of the linear (for $B = 0$ T) and circular (for $B > 0$ T) polarization state of the NW luminescence was accomplished by using a linear polarizer and a liquid crystal variable retarder suitably combined to make all measurements insensitive to the polarization response of the optical setup. All PL spectra were normalized by the setup responses. The magnetic field was either directed orthogonal (Voigt configuration) or parallel (Faraday configuration) to the emitted light wavevector k. Backscattering configuration was used in both geometries. The laser and luminescence emission traveled in opposite directions and both were orthogonal to the sample substrate, namely, parallel to the long axis (*i.e.*, $\hat{c}$) of the NWs.

Conflict of Interest: The authors declare no competing financial interest.

Acknowledgment. Useful discussions with Prof. A. L. Efros are gratefully acknowledged. Part of this work has been supported by EuroMagNET II under EU Contract No. 228043. We acknowledge the support of the HFML-RU/FOM, member of the European Magnetic Field Laboratory (EMFL).

Note Added after ASAP Publication: This paper posted ASAP on December 2, 2013. Due to a production error, an equation in the Results and Discussion section was corrected and the revised version was reposted on December 5, 2013.

REFERENCES AND NOTES

1. Yan, R.; Gargas, D.; Yang, P. Nanowire Photonics. *Nat. Photonics* **2009**, *3*, 569–576.
2. Yang, P.; Yan, R.; Fardy, M. Semiconductor Nanowire: What's Next?. *Nano Lett.* **2010**, *10*, 1529–1536.
3. Shtrikman, H.; Popovitz-Biro, R.; Kretinin, A.; Houben, L.; Heiblum, M.; Bukała, M.; Galicka, M.; Buczko, R.; Kacman, P. Method for Suppression of Stacking Faults in Wurtzite III-V Nanowires. *Nano Lett.* **2009**, *9*, 1506–1510.
4. De Luca, M.; Lavenuta, G.; Polimeni, A.; Rubini, S.; Grillo, V.; Mura, F.; Miriametro, A.; Capizzi, M.; Martelli, F. Excitonic Recombination and Absorption in $In_xGa_{1-x}As$/GaAs Heterostructure Nanowires. *Phys. Rev. B* **2013**, *87*, 235304 and references therein.
5. Birman, J. L. Polarization of Fluorescence in CdS and ZnS Single Crystals. *Phys. Rev. Lett.* **1959**, *2*, 157–159.
6. Zanolli, Z.; Fuchs, F.; Furthmüller, J.; von Bart, U.; Bechstedt, F. Model GW Band Structure of InAs and GaAs in the Wurtzite Phase. *Phys. Rev. B* **2007**, *75*, 245121.
7. De, A.; Pryor, C. E. Predicted Band Structures of III-V Semiconductors in the Wurtzite Phase. *Phys. Rev. B* **2010**, *81*, 155210.
8. Cheiwchanchamnangij, T.; Lambrecht, W. R. L. Band Structure Parameters of Wurtzite and Zinc-Blende GaAs under Strain in the GW Approximation. *Phys. Rev. B* **2011**, *84*, 035203.
9. Assali, S.; Zardo, I.; Plissard, S.; Kriegner, D.; Verheijen, M. A.; Bauer, G.; Meijerink, A.; Belabbes, A.; Bechstedt, F.; Haverkort, J. E. M.; *et al.* M. Direct Band Gap Wurtzite Gallium Phosphide Nanowires. *Nano Lett.* **2013**, *13*, 1559–1563.
10. Ketterer, B.; Heiss, M.; Uccelli, E.; Arbiol, J.; Fontcuberta i Morral, A. Untangling the Electronic Band Structure of Wurtzite GaAs Nanowires by Resonant Raman Spectroscopy. *ACS Nano* **2011**, *5*, 7585–7592.
11. A. Mishra, A.; Titova, L. V.; Hoang, T. B.; Jackson, H. E.; Smith, L. M.; Yarrison-Rice, J. M.; Kim, Y.; Joyce, H. J.; Gao, Q.; Tan, H. H.; *et al.* Polarization and Temperature Dependence of Photoluminescence from Zincblende and Wurtzite InP Nanowires. *Appl. Phys. Lett.* **2007**, *91*, 263104.
12. Fang, L.; Zhao, X.; Chiu, Y. -H.; Ko, D.; Reddy, K. M.; Lemberger, T. R.; Padture, N. P.; Yang, F. Comprehensive Control of Optical Polarization Anisotropy in Semiconducting Nanowires. *Appl. Phys. Lett.* **2011**, *99*, 14110.
13. Gadret, E. G.; Dias, G. O.; Dacal, L. C. O.; de Lima, M. M., Jr.; Ruffo, C. V. R. S.; Iikawa, F.; Brasil, M. J. S. P.; Chiaramonte, T.; Cotta, M. A.; Tizei, L. H. G.; *et al.* Valence-Band Splitting Energies in Wurtzite InP Nanowires: Photoluminescence Spectroscopy and *Ab Initio* Calculations. *Phys. Rev. B* **2010**, *82*, 125327.
14. Kim, D. C.; Dheeraj, D. L.; Fimland, B. O.; Weman, H. Polarization Dependent Photocurrent Spectroscopy of Single Wurtzite GaAs/AlGaAs Core-Shell Nanowires. *Appl. Phys. Lett.* **2013**, *102*, 142107.
15. Kusch, P.; Breuer, S.; Ramsteiner, M.; Geelhar, L.; Riechert, H.; Reich, S. Band Gap of Wurtzite GaAs: A Resonant Raman Study. *Phys. Rev. B* **2012**, *86*, 075317.
16. Tronc, P.; Kitaev, Yu. E.; Wang, G.; Limonov, M. F.; Panfilov, A. G.; Neu, G. Optical Selection Rules for Hexagonal GaN. *Phys. Status Solidi B* **1999**, *216*, 599–603.
17. Plochocka, P.; Mitoglu, A. A.; Maude, D. K.; Rikken, G. L. J. A.; Granados del Aguila, A.; Christianen, P. C. M.; Kacman, P.; Shtrikman, H. High Magnetic Field Reveals the Nature of Excitons in a Single GaAs/AlAs Core/Shell Nanowire. *Nano Lett.* **2013**, *13*, 2442–2447.
18. Corfdir, P.; Van Hattem, B.; Uccelli, E.; Conesa-Boj, S.; Lefebvre, P.; Fontcuberta i Morral, A.; Phillips, R. T.

Three-Dimensional Magneto-Photoluminescence as a Probe of the Electronic Properties of Crystal-Phase Quantum Disks in GaAs Nanowires. *Nano Lett.* **2013**, *13*, 5003–5310.
19. Oh, E.; Choi, J. H.; Oh, D. K.; Park, J. Magnetophotoluminescence and Energy-Dependent Circular Polarization from CdMnS Nanowires. *Appl. Phys. Lett.* **2008**, *93*, 041911.
20. Wojnar, P.; Janik, E.; Baczewski, L. T.; Kret, S.; Dynowska, E.; Wojciechowski, T.; Suffczyński, J.; Papierska, J.; Kossacki, P.; Karczewski, G.; *et al.* Giant Spin Splitting in Optically Active ZnMnTe/ZnMgTe Core/Shell Nanowires. *Nano Lett.* **2012**, *12*, 3404–3409.
21. Thomas, D. G.; Hopfield, J. J. Exciton Spectrum of Cadmium Sulfide. *Phys. Rev.* **1959**, *116*, 573–582.
22. Wheeler, R. G; Dimmock, J. O. Exciton Structure and Zeeman Effects in Cadmium Selenide. *Phys. Rev.* **1962**, *125*, 1805–1815.
23. Cho, K. Unified Theory of Symmetry-Breaking Effects on Excitons in Cubic and Wurtzite Structures. *Phys. Rev. B* **1976**, *14*, 4463–4482.
24. Broser, I.; Rosenzweig, M. Determination of Excitonic Parameters of the A Polariton of CdS from Magnetoreflectance Spectroscopy. *Phys. Rev. B* **1980**, *22*, 2000–2007.
25. Rodina, A. V.; Dietrich, M.; Göldner; Eckey, L.; Hoffmann, A.; Efros, Al. L.; Rosen, M.; Meyer, B. K. Free Excitons in Wurtzite GaN. *Phys. Rev. B* **2001**, *64*, 115204.
26. Furis, M.; Hollingsworth, J. A.; Klimov, V. I.; Crooker, S. A. Time- and Polarization-Resolved Optical Spectroscopy of Colloidal CdSe Nanocrystal Quantum Dots in High Magnetic Fields. *J. Chem. Phys.* **2005**, *109*, 15332–15333.
27. Venghaus, H.; Suga, S.; Cho, K. Magnetoluminescence and Magnetoreflectance of the A Exciton of CdS and CdSe. *Phys. Rev. B* **1977**, *16*, 4419–4428.
28. Ulbrich, R. G.; Weisbuch, C. Resonant Brillouin Scattering of Excitonic Polaritons in Gallium Arsenide. *Phys. Rev. Lett.* **1977**, *38*, 865–868.
29. Jabeen, F.; Rubini, S.; Grillo, V.; Martelli, F. InGaAs/GaAs Core-Shell Nanowires Grown by Molecular Beam Epitaxy. *IEEE J. Sel. Top. Quantum Electron.* **2011**, *17*, 794–800.
30. Jabeen, F.; Rubini, S.; Martelli, F. Growth of III-V Semiconductor Nanowires by Molecular Beam Epitaxy. *Microelectron. J.* **2009**, *40*, 442–445.
31. Bao, J.; Bell, D. C.; Capasso, F.; Wagner, J. B.; Martensson, T.; Tragardh, J.; Samuelson, L. Optical Properties of Rotationally Twinned InP Nanowire Heterostructures. *Nano Lett.* **2008**, *8*, 836–841.
32. Pemasiri, K.; Montazeri, M.; Gass, R.; Smith, L. M.; Jackson, H. E.; Yarrison-Rice, J.; Paiman, S.; Gao, Q.; Tan, H. T.; Jagadish, C.; *et al.* Carrier Dynamics and Quantum Confinement in type II ZB-WZ InP Nanowire Homostructures. *Nano Lett.* **2009**, *9*, 648–654.
33. Fang, L.; Zhao, X.; Chiu, Y.-H.; Ko, D.; Kongara, M. R.; Lemberger, T. R.; Padture, N. P.; Yang, F.; Johnston-Halperin, E. Comprejensive Control of Optical Polarization Anisotropy in Semiconducting Nanowires. *Appl. Phys. Lett.* **2011**, *99*, 141101.
34. MacDonald, A. H.; Ritchie, D. S. Hydrogenic Energy Levels in Two Dimensions at Arbitrary Magnetic Fields. *Phys. Rev. B* **1986**, *33*, 8336–8344.
35. Atanasov, R.; Bassani, F.; D'Andrea, A.; Tomassini, N. Exciton Properties and Optical Response in $In_xGa_{1-x}As$/GaAs Strained Quantum Wells. *Phys. Rev. B* **1994**, *50*, 14381–14388.
36. Cabib, D.; Fabri, E.; Fiorio, G. Ground and First Excited States of Excitons in a Magnetic Field. *Il Nuovo Cimento* **1972**, *10 B*, 185–199.
37. Zhang, Y.; Mascarenhas, A.; Jones, E. D. Magnetoexcitons in Anisotropic Semiconductors. *J. Appl. Phys.* **1998**, *83*, 448–454.
38. Pettinari, G.; Polimeni, A.; Masia, F.; Trotta, R.; Felici, M.; Capizzi, M.; Niebling, T.; Stolz, W.; Klar, P. J. Electron Mass in Dilute Nitrides and its Anomalous Dependence on Hydrostatic Pressure. *Phys. Rev. Lett.* **2007**, *98*, 146402.
39. Thomas, D. G.; Hopfield, J. J. Bound Exciton Complexes. *Phys. Rev. Lett.* **1961**, *7*, 316–319.
40. Prof. Al L. Efros; private communication.
41. Efros, A. L. In *Semiconductor and Metal Nanocrystals*; Klimov, V. I., Ed.; Marcel Dekker Inc.: New York, 2004.
42. Röseler, J.; Henneberger, K. Magnetopolaritions in Wurtzite-Type Ctystals. *Phys. Status Solidi B* **1979**, *93*, 213–222.
43. Chamarro, M. A.; Gourdon, C.; Lavallard, P. Optical Pumping in $CdS_{1-x}Se_x$. *Semicond. Sci. Technol.* **1993**, *8*, 1868–1874.
44. Johnston-Halperin, E.; Awschalom, D. D.; Crooker, S. A.; Efros, A. L.; Rosen, M.; Peng, X.; Alivisatos, P. Spin Spectroscopy of Dark Excitons in CdSe Quantum Dots to 60 T. *Phys. Rev. B* **2001**, *63*, 205309.
45. Hümmer, K. Interband Magnetoreflection of ZnO. *Phys. Status Solidi C* **1973**, *56*, 249–260.
46. Yeh, C.-Y.; Wei, S.-H.; Zunger, A. Relationships Between the Band Gaps of the Zinc-Blende and Wurtzite Modifications of Semiconductors. *Phys. Rev. B* **1994**, *50*, 2715–2718.
47. Wijnen, F. J. P.; Blokland, J. H.; Chin, P. T. K.; Christianen, P. C. M.; Maan, J. C. Competition between Zero-Phonon and Phonon-Assisted Luminescence in Colloidal CdSe Quantum Dots. *Phys. Rev. B* **2008**, *78*, 235318.
48. Traynor, N. J.; Warburton, R. J.; Snelling, M. J.; Harley, R. T. Highly Nonlinear Zeeman Splitting of Excitons in Semiconductor Quantum Wells. *Phys. Rev. B* **1997**, *55*, 15701.
49. Jadczak, J.; Kubisa, M.; Ryczkp, K.; Bryja, L.; Potemski, M. High Magnetic Field Spin Splitting of Excitons in Asymmetric GaAs Quantum Wells. *Phys. Rev. B* **2012**, *86*, 245401.
50. Nam, S. B.; Reynolds, D. C.; Litton, C. W.; Almassy, R. J.; Collins, T. C.; Wolfe, C. M. Free-Exciton Energy Spectrum in GaAs. *Phys. Rev. B* **1976**, *13*, 761–767.
51. Wysmolek, A.; Potemski, M.; Stepniewski, R.; Lusakowski, J.; Pakula, K.; Baranowski, J. M.; Martinez, G.; Wyder, P.; Grzegory, I.; Porowski, S. Polarised Magnetoluminescence of Excitons in Homoepitaxial GaN Layers. *Phys. Status Solidi B* **1999**, *216*, 11–15.
52. *Landolt-Börnstein, Numerical Data and Functional Relationship in Science and Technology*; Rössler, U., Eds.; Springer-Verlag: Berlin, 1987.
53. Efros, A. L. In *Semiconductor and Metal Nanocrystals*; Klimov, V. I., Ed.; Marcel Dekker Inc.: New York, 2004.
54. Baldassarri Höger von Högersthal, G.; Polimeni, A.; Masia, F.; Bissiri, M.; Capizzi, M.; Gollub, D.; Fischer, M.; Forchel, A. Magnetophotoluminescence Studies of (InGa)(AsN)/GaAs Heterostructures. *Phys. Rev. B* **2003**, *67*, 233304 (2003).
55. Jancu, J.-M.; Gauthron, K.; Largeau, L.; Patriarche, G.; Harmand, J.-C.; Voisin, P. Type II Heterostructures Formed by Zinc-Blende Inclusions in InP and GaAs Wurtzite Nanowires. *Appl. Phys. Lett.* **2010**, *97*, 041910.